IEEE Robotics and Automation Letters (RAL) paper presented at
2024 IEEE/RSJ International Conference on Intelligent Robots and Systems (IROS)
October 14-18, 2024. Abu Dhabi, UAE

Hierarchical Trajectory Deformation Algorithm with Hybrid Controller for Active Lower Limb Rehabilitation

Ze Yang[1], Hu Jin[1], Wei Gao[1], Erlong Wang[1], Yang Shu[1], Ming Wu[2] and Shiwu Zhang[1]

***Abstract*—Robot-aided active rehabilitation has shown to be an effective treatment approach for hemiplegic patients. This paper presents an active control framework for lower limb rehabilitation, combining an interaction layer with a hierarchical trajectory deformation algorithm (HTDA), and an assist-as-needed (AAN) layer with a hybrid controller. The HTDA uses constrained optimization in both position and velocity domains to continuously generate smooth reference trajectories based on virtual interaction forces during physical human-robot interaction (pHRI). An additional optimization loop is also implemented to achieve adaptive parameter adjustment for HTDA. Meanwhile, the hybrid controller relies on a force field term and a velocity field term to provide AAN feature. The proposed method is validated on a two-degree-of-freedom lower limb rehabilitation robot for walking with variable step height and step length. The experimental results demonstrate that compared to previously developed admittance model (AM) and trajectory deformation algorithm (TDA), under four different evaluation metrics, HTDA can improve dimensionless squared jerk (DSJ) by 73.6% comparing to AM and improve constraint force percentage (CFP) by 20.4% comparing to TDA. This demonstrate the effectiveness of the proposed framework in reducing human-robot confrontation, especially in improving robot actuation compliance and movement smoothness.**

***Index Terms*—Physical human-robot interaction (pHRI), rehabilitation robotics, hierarchical trajectory deformation algorithm, active rehabilitation.**

I. Introduction

STROKE is the third leading cause of chronic physical disability, with 70% to 80% of stroke patients lose the ability to live independently, primarily due to lower limb functional impairment [1], [2]. Gait training plays a pivotal role in rehabilitating lower limb motor function after a stroke [3]. Consequently, a variety of lower limb rehabilitation robots (LLRRs), such as LOKOMAT, REWALK and ALEX [4], [5], [6], have been extensively used in the training processes. Among them, LLRRs with passive control strategies are commonly used for early-stage rehabilitation of stroke patients [7]. Such strategies have made the control of rehabilitation relatively simple and effective. However, the lack of interaction between the robot and the patients hinders its further application, because only active training can induce the neural plasticity needed for rehabilitation [8]. Therefore, an active controller with assist-as-needed (AAN) property can have a better prospect.

Constructing an active controller with AAN property involves assessing the patient's functional needs and implementing the corresponding assistance [9]. Caulcrick et al. [10] utilized electromyographic (EMG) signals measured from the patient's healthy side to guide the active rehabilitation of the impaired side. Pehlivan et al. [11] estimated the patient's input through a model-based disturbance observer, and calculated the required compensation torque to achieve the desired motion. Another general technique to develop active rehabilitation is to construct either a force field controller [12], [6] or a velocity field controller [13], [14]. Within this context, Cao *et al.* validated the stability of a force field controller using Lyapunov methods [15], while Zhang *et al.* achieved parameter adaptation of a force field controller through a learning-based approach [16]. However, once the real trajectory deviates from the reference trajectory by a relatively large distance, the robot may exert excessive constraint forces on the patient, leading to discomfort and unnatural movement. Introducing physical human-robot interaction (pHRI) algorithm in the controller can solve this problem. For instance, Asl *et al.* improved their robot's compliance by adding admittance model (AM) [17] into their controller through force and velocity field terms [18]. However, as a second-order interaction model, Ferraguti *et al.* [19] pointed out that AM can induce higher-order disturbances. This compromises the robot's movement stability, posing safety risks. Besides, the reference trajectory generated by the AM-based controller only contains one point, such that the corresponding trajectory may possess a poor continuity and further limit the rehabilitation performance.

Recently, Zhou *et al.* [20] and Yang *et al.* [21] applied trajectory deformation algorithm (TDA) [22] to generate smooth

Manuscript received: January 9, 2024; Revised: March 23, 2024; Accepted: April 24, 2024.

This paper was recommended for publication by Editor Pietro Valdastri upon evaluation of the Associate Editor and Reviewers' comments. This work was supported by grants from the National Natural Science Foundation of China under Nos. U21A20119, 51705495 and 62103395, the Natural Science Foundation of Anhui Province of China under No. 2008085UD02, the Anhui Provincial Key Research and Development Program under No. 202104h04020004, the Anhui Provincial Major Science and Technology Project under No. 202203107020016, and the USTC-Anhui Aibo Intelligent Robot Joint Laboratory. (Corresponding authors: Hu Jin; Wei Gao.)

This work involved human subjects in its research. Approval of all ethical and experimental procedures and protocols was granted by Anhui Provincial Hospital Ethics Committee under Application No. 2023KY-348.

[1]Ze Yang, Hu Jin, Wei Gao, Erlong Wang, Yang Shu and Shiwu Zhang are with the CAS Key Laboratory of Mechanical Behavior and Design of Materials, Department of Precision Machinery and Precision Instrumentation, University of Science and Technology of China, Hefei, Anhui 230027, China. jhrdsp@ustc.edu.cn; weigao@ustc.edu.cn.

[2]Ming Wu is with the First Affiliated Hospital of USTC, Division of Life Sciences and Medicine, University of Science and Technology of China, Hefei, Anhui, 230001, China.

Digital Object Identifier (DOI): see top of this page.

This article has been accepted for publication in IEEE Robotics and Automation Letters. This is the author's version which has not been fully edited and content may change prior to final publication. Citation information: DOI 10.1109/LRA.2024.3396369

reference trajectories during interaction, which was able to guide the robot to achieve active rehabilitation with lower energy consumption. However, they only discussed the relationship between the interaction force and the corresponding trajectory deformation in the position domain, which hinders TDA's response speed for active interaction and can result in an abnormal increase in the interaction force. In addition, the parameters of the TDA proposed in [20] and [22] are fixed, that is, the relationship between the interaction force and the trajectory deformation is fixed, which may become ineffective in complex human-robot interaction tasks.

Therefore, this paper attempts to improve the response speed of TDA and its stability at the same time. An active control framework with an interaction layer and an assist-as-needed layer is proposed. The interaction layer utilizes a hierarchical trajectory deformation algorithm (HTDA) to improve the robot's response speed to human interaction. Compared to conventional TDA methods, HTDA uses separate constrained optimization in both position and velocity domains to generate a smooth reference trajectory while the human is interacting with the robot, aiming to mitigate the confrontation in between. Additionally, an extra optimization loop enabling parameter adjustment for HTDA based on variable interaction forces is added to further improve HTDA's adaptability. On the other hand, the AAN layer employs a hybrid controller to constrain the human motion to the reference trajectory and provide adjustable assistance. The framework is verified through experiments conducted on a two-degree-of-freedom (2-DoF) LLRR with the participation of six healthy human subjects. The main contributions of this paper can be summarized as follows:

1) A human-robot interaction control framework with a novel HTDA within its interaction layer is proposed. HTDA's dual-domain trajectory optimization and adaptive parameter adjustment enable responsive and stable human-robot interaction under this framework.

2) Preliminary verification of the proposed framework is conducted with six healthy human subjects. The experimental results demonstrate the effectiveness of HTDA over conventional methods, such as AM and TDA, in handling physical human-robot interaction. HTDA helps yield a more compliant rehabilitation robot and a series of smoother rehabilitation motion.

NOMENCLATURE

f_v, f_{ext}	Virtual and measured actual interaction forces
f_t, f_n	Orthogonal components of f_v
$\ddot{q}$, $\dot{q}, q$	Vectors of joint acceleration, velocity and position
t_s, t_e	Time at which current trajectory deformation starts and ends
δ	Sampling period
N	Number of sampling points between t_s and t_e
Γ_d, Y_d	Desired position and velocity of the reference trajectory between t_s and t_e
$\tilde{\Gamma}_d$, $\tilde{Y}_d$	Deformation of Γ_d and Y_d
H, H_m	Deformation vectors of Γ_d and Y_d
μ, μ_m	Admittance gain of the deformation vectors
f	Operating frequency
F_n, F_t	Force field and velocity field control vectors
τ_r, τ_f	Gravity and friction compensation torques
τ_a, τ_{out}	Assistive torque exerted by the robot on the human body, total output torque of the robot

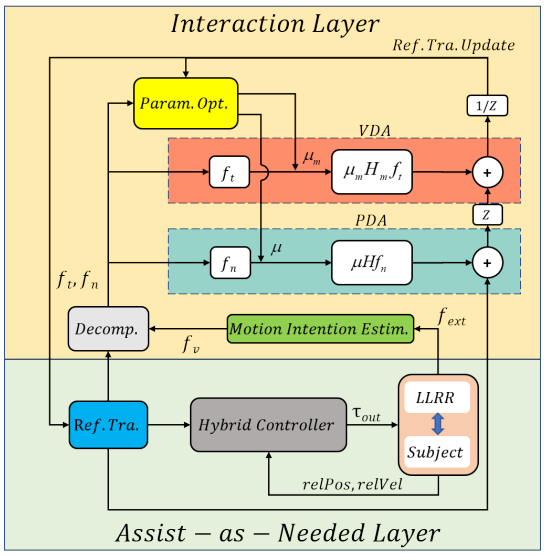

Fig. 1. Diagram of the proposed active control framework.

II. METHODS

This section describes the proposed control framework as shown in Fig. 1. As mentioned, the framework consists of the interaction layer and the assist-as-needed layer.

A. The Interaction Layer

The interaction layer contains a velocity deformation algorithm (VDA) module, a position deformation algorithm (PDA) module, a parameter optimization module and a motion intention estimation and decomposition module. The former three contributes to the proposed HTDA in this paper. As with the motion intention estimation and decomposition module, previous studies have shown that by either combining biological signals with musculoskeletal models or integrating motion information with dynamic models, it is possible to estimate the subject's motion intention using the interaction forces [23]. Therefore, referring to [24] and [25], this work calculates the virtual interaction force (VIF) using the dynamic model-based approach and treats it as the subject's motion intention. The model-based virtual interaction force can be calculated as

$$f_v = J^{-T}(J^T f_{ext} - \tau_a) \tag{1}$$

$$\tau_a = K_a(M_h(q)\ddot{q} + C_h(q,\dot{q})\dot{q} + G_h(q)) \tag{2}$$

$$f_t = f_v \cdot \frac{V(t_s)}{\|V(t_s)\|} \tag{3}$$

$$f_n = f_v - f_t \tag{4}$$

where J is the Jacobian matrix of the mapping between the joint positions and the ankle positions of the subject,

This article has been accepted for publication in IEEE Robotics and Automation Letters. This is the author's version which has not been fully edited and content may change prior to final publication. Citation information: DOI 10.1109/LRA.2024.3396369

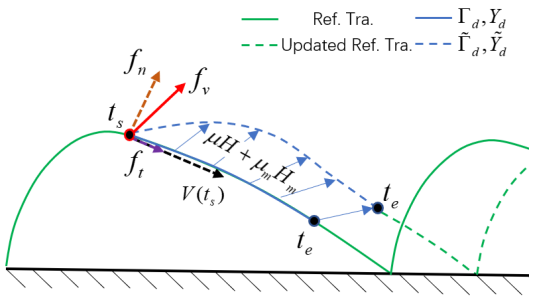

Fig. 2. Diagram of the reference trajectory deformation. The blue solid line represents the original trajectory and the blue dashed line is the deformed trajectory.

$K_a \in [0,1]$ is used to adjust the desired torque that the LLRR should provide to the subject, $M_h(q)$, $C_h(q,\dot{q})$ and $G_h(q)$ are the inertia matrix, the centrifugal and Coriolis matrix, and the gravity vector of the subject, respectively, $V(t_s)$ is the velocity vector of the reference trajectory at the time t_s. Since f_{ext} can be directly measured, there is no need to design additional observers.

Typically, the robot's active response to the subject's motion intention is realized by generating an updated reference trajectory accordingly [26]. With the calculated physical human-robot interaction force, Fig. 2 illustrates a typical reference trajectory deformation under HTDA, resulted from the combined effort of VDA and TDA.

1) Velocity deformation algorithm: VDA is used to handle the tangential interaction force with respect to the reference trajectory. Referring to [22] and [27], the interaction forces can be assumed to remain unchanged for a certain period of time after human-robot interaction. To obtain the optimal velocity deformation, the energy of tangential velocity deformation is defined as

$$\begin{aligned} E(\tilde{Y}_d) = E(Y_d) + (\tilde{Y}_d - Y_d)(-\hat{F}_t^T)T^T \\ + \frac{1}{2\alpha}(\tilde{Y}_d - Y_d)^T R(\tilde{Y}_d - Y_d) \end{aligned} \tag{5}$$

with

$$\begin{cases} \hat{F}_t = f_t(t_s)\vec{1} \\ R = A^T A \in \mathbb{R}^{N\times N} \\ A = \begin{bmatrix} 1 & 0 & 0 & & 0 \\ -3 & 1 & 0 & & 0 \\ 3 & -3 & 1 & \cdots & 0 \\ -1 & 3 & -3 & & 0 \\ 0 & -1 & 3 & & 0 \\ 0 & 0 & -1 & & 0 \\ & \vdots & & \ddots & \vdots \\ 0 & 0 & 0 & & 1 \\ 0 & 0 & 0 & & -3 \\ 0 & 0 & 0 & \cdots & 3 \\ 0 & 0 & 0 & & -1 \end{bmatrix} \in \mathbb{R}^{(N+3)\times N} \end{cases}$$

where $\hat{F}_t$ is the force representing the subject's motion intention tangential to the reference trajectory, $f_t(t_s)$ is the actual value calculated at the time t_s, $\vec{1} \in \mathbb{R}^{1\times N}$ is a vector with all elements being one, R is a symmetric positive definite matrix, and A is a matrix calculated as the third derivative of velocity deformation. In (5), the first term is the undeformed velocity's energy, the second term enables $\hat{F}_t$ to affect the deformed velocity's energy, and the third term allows the deformation to have minimum jerk.

To achieve a smooth transition from current reference velocity to a new reference velocity, the first two and the last two waypoints of $\tilde{Y}_d$ need to be the same as those of Y_d. Meanwhile, the system should also ensure conservation of momentum, thus an optimization problem can be set as

$$\begin{aligned} &\text{min: } E(\tilde{Y}_d) \\ &\text{s.t.} \begin{cases} B(\tilde{Y}_d - Y_d) = 0 \\ K_m\vec{1}(\tilde{Y}_d - Y_d) - \hat{F}_t^T(\delta\vec{1})^T = 0 \end{cases} \end{aligned} \tag{6}$$

with

$$B = \begin{bmatrix} 1 & 0 & 0 & \cdots & 0 & 0 & 0 \\ 0 & 1 & 0 & \cdots & 0 & 0 & 0 \\ 0 & 0 & 0 & \cdots & 0 & 1 & 0 \\ 0 & 0 & 0 & \cdots & 0 & 0 & 1 \end{bmatrix} \in \mathbb{R}^{4\times N}$$

where K_m is a positive constant. As demonstrated in [28], (6) can be straightforwardly solved through the method of Lagrange multipliers, with the Lagrangian being defined as

$$\begin{aligned} L(\tilde{Y}_d, \lambda_1, \lambda_2) = E(Y_d) + \lambda_1 B(\tilde{Y}_d - Y_d) \\ + \lambda_2(K_m\vec{1}(\tilde{Y}_d - Y_d) - \hat{F}_t^T(\delta\vec{1})^T) \end{aligned} \tag{7}$$

where λ_1 and λ_2 are vectors of Lagrange multipliers. By solving (7), the finial equations for VDA are

$$\begin{cases} \tilde{Y}_d = Y_d + \mu_m H_m f_t(t_s) \\ H_m = \dfrac{\delta P}{f(N+1)\|P\|} \end{cases} \tag{8}$$

with

$$\begin{cases} P = (\beta I - M^T(MZM^T)^{-1}(\vec{1} - \beta MR^- Z))\vec{1} \\ Z = (I - R^- B^T(BR^- B^T)^- B)R^- \vec{1} \\ \beta = \frac{1}{\|Z\|}, I \in \mathbb{R}^{N\times N}, \vec{1} \in \mathbb{R}^N \end{cases}$$

Fig. 3 shows the curve of H_m under different parameter sets. Comparing (8) to [22, eq.(29)], the number of time steps N is placed in the denominator to cause the magnitude of H_m to decrease as N increases. On the other hand, the frequency f is introduced in the denominator to cause the magnitude of H_m to decrease as f increases. Both setups aim to achieve similar performance of the algorithm under different N and f combinations, and make μ_m the primary factor controlling the algorithm's compliance.

2) Position deformation algorithm: PDA is used to handle the normal interaction force with respect to the reference trajectory. Using the same method, the energy of normal trajectory deformation is defined as

$$\begin{aligned} E(\tilde{\Gamma}_d) = E(\Gamma_d) + (\tilde{\Gamma}_d - \Gamma_d)(-\hat{F}_n) \\ + \frac{1}{2\alpha}(\tilde{\Gamma}_d - \Gamma_d)^T R(\tilde{\Gamma}_d - \Gamma_d) \end{aligned} \tag{9}$$

This article has been accepted for publication in IEEE Robotics and Automation Letters. This is the author's version which has not been fully edited and content may change prior to final publication. Citation information: DOI 10.1109/LRA.2024.3396369

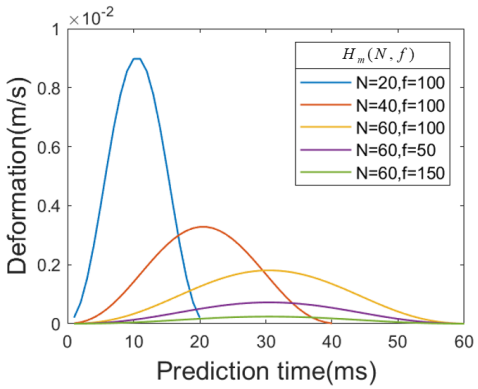

Fig. 3. Shapes of H_m under different parameter combinations.

where $\hat{F}_n = f_n(t_s)\vec{1}$ is the force representing the subject's motion intention normal to the reference trajectory, and $f_n(t_s)$ is the actual value calculated at the time t_s. Similar to (6), we can formulate the optimization problem as

$$\begin{aligned} &\text{min: } E(\tilde{\Gamma}_d) \\ &\text{s.t. } B(\tilde{\Gamma}_d - \Gamma_d) = 0 \end{aligned} \tag{10}$$

For brevity, the similar derivation process is skipped here, and the finial equations for PDA are expressed as

$$\begin{cases} \tilde{\Gamma}_d = \Gamma_d + \mu H f_n(t_s) \\ H = \dfrac{\delta Z}{f(N+1)\|Z\|} \end{cases} \tag{11}$$

It is worth noting that when HTDA takes effect, the reference trajectory undergoes permanent global deformation as shown in Fig. 2 to reduce human-robot confrontation, thereby reducing unnecessary interaction forces. Comparing to TDA, HTDA uses VDA instead of PDA in the tangential direction to achieve this global deformation, while keeps the PDA used in the normal direction to avoid excessive deviation from the original reference trajectory. Otherwise, like the TDA method in [22], only local trajectory deformation can be generated, while a global deformation required by the subject would require the subject's continuous and increased effort through interaction.

3) Parameter optimization: As HTDA improves the robot's compliance, the subject can modify the LLRR's original movement with smaller interaction force. This improves the subject's comfort in pHRI. Based on (8) and (11), the compliance of the LLRR using HTDA can be adjusted by changing μ, μ_m, H and H_m. Due to the complex forms of H and H_m, changing μ and μ_m is simpler and more efficient in real-time application. Therefore, μ and μ_m are adjusted by solving the following optimization problem:

$$\begin{aligned} \min_{u,\mu_m}\ & \frac{\sum_{i=0}^{N}(W_i^T Q_r W_i + F_{t_i}^T Q_{f_t} F_{t_i} + F_{n_i}^T Q_{f_n} F_{n_i})}{N+1} \\ \text{s.t.}\quad & lb \le \mu, \mu_m \le ub \end{aligned} \tag{12}$$

where W_i represents additional torque output from the LLRR, F_{t_i} and F_{n_i} represent anticipated tangential and normal interaction force at the i-th predicted time step. The first term in the summation represents the extra energy cost of LLRR in dealing with pHRI, and the second and the third terms are the interaction costs in the tangential and normal directions, respectively. Q_r, Q_{f_t} and Q_{f_n} are weight matrices that are designed as positive definite diagonal matrices to ensure optimization convergence. In addition, the output of μ and μ_m are constrained within lower bound lb and upper bound ub to ensure that the effect of parameter variation on the position and velocity deformation is limited.

Because W_i in the first term of (12) can be approximated using the first-order Taylor expansion, we can have

$$\begin{cases} W_i = \dfrac{\Delta W_i}{\|W_{i_0}\|},\ W_{i_0} = A_t Q_t + G_0 \\ \Delta W_i = A_t \begin{pmatrix} S_i D H_m f_t & S_i D D H f_n \\ S_i H_m f_t & S_i D H f_n \\ S_i D^- H_m f_t & S_i H f_n \end{pmatrix} \begin{pmatrix} \mu_m \\ \mu \end{pmatrix} \end{cases} \tag{13}$$

with

$$\begin{cases} A_t = \begin{pmatrix} M_0 J_0^- & C_0 J_0^- - J_0^{-T} d J_0 J_0^- & d G_0 J_0^- \end{pmatrix} \\ Q_t = \begin{pmatrix} \ddot{q}_i & \dot{q}_i & \Delta q \end{pmatrix}^T \end{cases}$$

where $S_i \in \mathbb{R}^{2\times N}$ is a matrix with all elements in the first i columns being 1, $D \in \mathbb{R}^{N\times N}$ is a derivative matrix, M_0, C_0, G_0 and J_0 are the inertia matrix, the centrifugal and Coriolis matrix, the gravity vector, and the the Jacobian matrix of the LLRR at initial time, respectively, dJ_0 and dG_0 are the first derivate of J_0 and G_0, respectively, and $\ddot{q}_i$, $\dot{q}_i$ and Δq are the acceleration, the velocity and the position variation of each joint at the i-th prediction time step, respectively.

Assuming that f_t and f_n will decrease with specific rate in future time, we have

$$\begin{cases} F_{ti} = \dfrac{J^- \hat{f}_{ti}}{\|J^- f_t\|},\ \hat{f}_{ti} = f_t - K_{\mu_m} S_i \mu_m H_m \\ F_{ni} = \dfrac{J^- \hat{f}_{ni}}{\|J^- f_n\|},\ \hat{f}_{ni} = f_n - K_\mu S_i \mu H \end{cases} \tag{14}$$

where K_μ and K_{μ_m} are the virtual stiffnesses that represent the hypothesized decreasing rates of the interaction force. Note that when the subject has strong lower limb motor abilities, Q_{f_t} and Q_{f_n} can be set to higher values, enabling the LLRR to respond quickly to the subject's motion intention. However, when the subject has weak lower limb strength, Q_{f_n} should be set to a lower value to ensure that the LLRR provides sufficient constraint to the subject's lower limb.

B. The Assist-As-Needed Layer

To utilize the reference trajectory generated by the interaction layer for active rehabilitation, field control approach has shown to be effective [14]. Therefore, inspired by [6] and [18], a hybrid controller is developed in this section, which applies the desired tangential and normal forces at the ankle of the subject. The normal force is provided by a position-dependent force field, which acts as a virtual wall around the reference trajectory, while the tangential force is provided by a velocity field, which helps move the ankle along the reference trajectory. Moreover, to enhance the transparency

This article has been accepted for publication in IEEE Robotics and Automation Letters. This is the author's version which has not been fully edited and content may change prior to final publication. Citation information: DOI 10.1109/LRA.2024.3396369

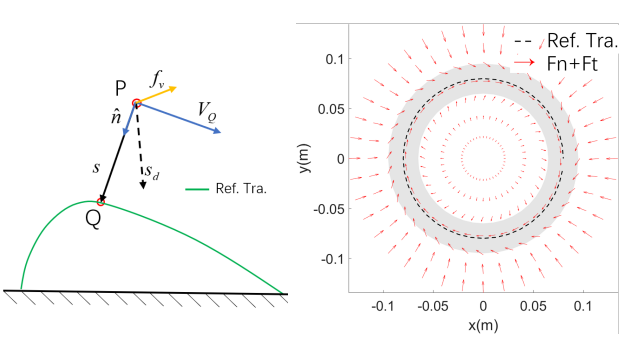

(a) (b)

Fig. 4. The construction of the force and velocity fields. (a) Diagram of intermediate quantities used in constructing the force and velocity fields. (b) The spatial distribution of the resultant vectors generated by the force and velocity fields.

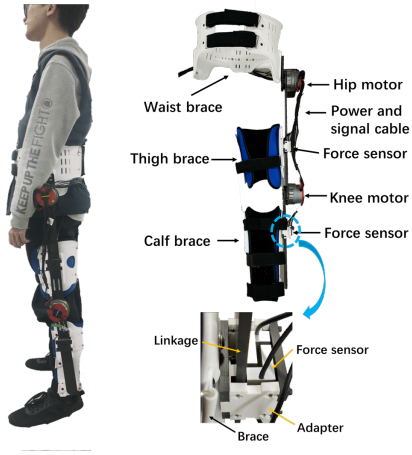

Fig. 5. Schematics of the 2-DoF LLRR.

of the control relationship, gravity compensation and friction compensation terms are incorporated into the hybrid controller.

The force field control vector F_n applies constraint forces to the subject based on position errors, which is described by

$$F_n = \begin{cases} [K_n(\frac{|s|-s_0}{s_n})^2 - K_{nd}\dot{s}]\hat{n}, & |\ s\ | > s_0 \\ 0, & \text{otherwise.} \end{cases} \tag{15}$$

where s denotes the distance from the ankle (point P in Fig. 4a) to the nearest point on the reference trajectory (point Q in Fig. 4a), $\hat{n}$ is a unit vector pointing from point P to Q, s_0 defines the boundary where F_n is ineffective, s_n is used to change the shape of F_n, and K_n and K_{nd} are positive constants resembling stiffness and damping parameters. When K_n is set to a higher value, the controller tends to prioritize correcting human motion rather than tolerating errors.

The velocity field control vector F_t provides assistive forces to the subject based on position error and reference velocity, which is defined as

$$F_t = \begin{cases} K_t V_Q e^{-k(\frac{|s|-s_0}{s_n})^2}, & |\ s\ | > s_0 \\ K_t V_Q, & \text{otherwise.} \end{cases} \tag{16}$$

where V_Q is the reference velocity of point Q, K_t is used to change the magnitude of the tangential force, e is the natural constant and k is a positively defined constant used to adjust the descending rate of F_t when the position error increases. It indicates that if current position is sufficiently close to the reference trajectory, then more control resources would be allocated to provide tangential force.

Fig. 4b illustrates the combination of velocity and force fields in the sagittal plane, where the gray region indicates F_n is ineffective, with its width being twice the value of s_0. Additionally, the hybrid controller also contains a damping force F_d, which is given by $F_d = K_d\dot{x}$ with K_d being a constant and $\dot{x}$ being the ankle's linear velocity. The resultant force applied at the ankle joint is given by the vector summation $F = F_n + F_t + F_d$. Note that the nonlinear dependency of F_n and F_t on s are used to constrain the position error and provide assistance. This nonlinearity ensures the assist-as-needed property and avoids performance degradation caused by single-term saturation. In actual deployment, it is important to have these variable weights to adjust each term within the summation.

On the other hand, in order to prevent the motion of the LLRR itself from affecting pHRI, compensation for the robot's dynamics and joint frictions are designed as

$$\tau_r = M(q)\ddot{q} + C(q,\dot{q})\dot{q} + G(q) \tag{17}$$

$$\tau_f = \tau_s \cdot sgn(\dot{q}) + \gamma\dot{q} \tag{18}$$

where $M(q)$, $C(q,\dot{q})$ and $G(q)$ are the inertia matrix, the centrifugal and Coriolis matrix, and the gravity vector of the LLRR, respectively, τ_s represents the static friction coefficient, and γ represents the dynamic friction coefficient. The final output of the hybrid controller takes the following form:

$$\tau_{out} = J^T F + \tau_a + \tau_r + \tau_f \tag{19}$$

III. Experiment

In this section, two sets of human-robot cooperative experiments are presented using a 2-DoF LLRR. Six human subjects participated in the experiments and completed both tasks. Experimental data have been evaluated using physical metrics and subjective questionnaires to show the effectiveness of the proposed methods in Section II.

A. The Lower Limb Rehabilitation Robot

As shown in Fig. 5, a 2-DoF LLRR was designed for active lower limb rehabilitation. Two motors (QDD Pro-PR60-100-80, mintasca, China) are installed at the hip joint and the knee joint, respectively. The rotation angles of the motors are limited within the ranges of human joint motion (hip joint: -15°$\sim$ 75°, knee joint: 0°$\sim$ 135°). One of the subject's lower limb is secured to the LLRR using thigh and calf braces, and the LLRR is fastened to the subject's waist through another brace. The interaction forces between the subject and the LLRR are measured by two 3D force sensors (CZ001, DECENT, China). These sensors are attached to the corresponding braces via adapters and measure the forces between the braces and the linkages connected to the actuation motors.

A slave MCU (STM32F767 core) is responsible for motor control and sensor information acquisition. A Linux-based master PC (an Intel NUC 10 with Core i7-10710U CPU) implements the proposed control framework in C++ language and communicates with the slave MCU to control the LLRR. In the experiments, the hybrid controller is operated at a higher frequency of 800 Hz due to its simplicity, while the HTDA is operated at 80 Hz for efficiency.

B. Evaluation Metrics

To evaluate the proposed control framework, this paper takes advantage of four evaluation metrics to compare its performance to other reference frameworks. These metrics include the energy per unit distance (EPUD), the dimensionless squared jerk (DSJ), the sum of applied torque (SAT) and the constraint force percentage (CFP).

EPUD can be considered as an index of robot compliance [29], DSJ evaluates the smoothness of a trajectory [20], SAT calculates the overall energy consumption by the controller, and CFP reflects the degree of human-robot confrontation. Their expressions are defined as

$$\text{EPUD} = \frac{\sum_{i=1}^{n} |f_v(t_i)\Delta d(t_i)|}{\sum_{i=1}^{n} |\Delta d(t_i)|} \tag{20}$$

$$\text{DSJ} = \int_{t_a}^{t_b} \dddot{x}(t)^2 dt \frac{(t_b - t_a)^5}{(x_{max} - x_{min})^2} \tag{21}$$

$$\text{SAT} = \int \|\tau_{out}(t)\| dt \tag{22}$$

$$\text{CFP} = \frac{\int \|J^{-T} F_n(t)\| dt}{\text{SAT}} \tag{23}$$

where $\Delta d(t_i)$ is the deviation from the reference trajectory to the deformed trajectory at time t_i, $\dddot{x}$ is the jerk of the trajectory, and t_a and t_b are the start time and the end time of a trajectory, respectively.

Intuitively, a lower EPUD value implies that the algorithm can better adapt to the subject's motion intention, which means higher robot compliance, a higher DSJ value implies that the trajectory is less smooth, which is unfavorable by the subject, a lower SAT value means that the LLRR can provide assistance with less energy consumption, and a smaller CFP value indicates less mismatch between the subject's movement and the LLRR's movement.

C. Experimental Setup

To emphasize the advantage of the proposed HTDA, the experiments have been designed to compare its performance in handling pHRI with previously developed TDA and AM inside the active control framework. As shown in the interaction layer of Fig. 6, when TDA is employed as the human-robot interaction algorithm instead of HTDA, the reference trajectory is updated directly using the virtual interaction force f_v. On the other hand, when AM is applied, it utilizes f_v and the actual trajectory deviation s from the hybrid controller to construct an admittance relationship, which can be described as

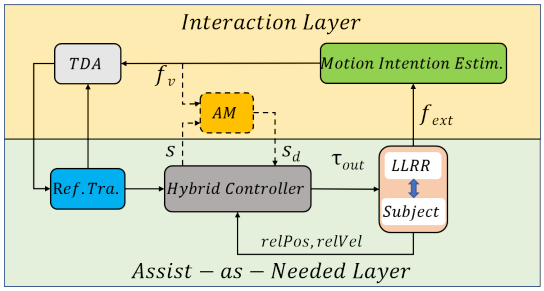

Fig. 6. The control framework with HTDA replaced by TDA or AM.

TABLE I
PARAMETER VALUES OF THE PROPOSED CONTROLLER

Symbol	Value	Units	Description
K_n	$diag$\{150,150\}	N	Force field gain
K_{nd}	$diag$\{10,10\}	N	Force field damp
K_t	$diag$\{50,50\}	$Nm^{-}s$	Velocity field gain
K_d	$diag$\{100,100\}	$Nm^{-}s$	End damping
C_d	$diag$\{5,5\}	$Nm^{-}s$	AM damping
C_s	$diag$\{100,100\}	Nm^{-}	AM stiffness
K_a	0.2	–	Assist level
N	60	–	Prediction length
δ	1.25	ms	sampling time
f	80	Hz	Operating frequency
μ, μ_m	{1,1,5,5}	–	HTDA admittance gain
Q_r	$diag$\{5,5\}	–	Weight matrix
Q_{f_n}, Q_{f_t}	$diag$\{50,50\}	–	Weight matrix

$$C_d(\dot{s}_d - \dot{s}) + C_s(s_d - s) = f_v \tag{24}$$

where C_d and C_s are the predefined damping and stiffness matrices, and s_d is the desired trajectory deviation. The parameters used in the active control framework are shown in Table 1.

Referring to selected segments of the CYBATHLON Exoskeleton Races in 2016 and 2020 [30], [31], two physical human-robot interaction experiments have been designed to assess the performance of the proposed active control framework, as illustrated in Fig. 7. In Exp. 1, the subjects were required to cross over obstacles on the ground along a pathway. In Exp. 2, the subjects were required to follow various markers on the ground with varying intervals. Typically, a human walking gait can be divided into swing phase and stance phase. During the stance phase, the LLRR only follows the movement of the subject, while during the swing phase, the LLRR was driven by the active control framework as described in Section II.

In both Exp. 1 and Exp. 2, three groups of experiments employing AM, TDA and HTDA as the human-robot interaction algorithm were conducted, respectively. Each group of experiment was repeated for six times with each subject. The four metrics given from (20) to (23) were calculated for each experiment. Additionally, NASA TLX was used to assess the task load for the subjects during the experiments [32]. A normality test with $p = 0.005$ and a t-test with $p = 0.05$ were used to confirm the validity of the experimental results.

This article has been accepted for publication in IEEE Robotics and Automation Letters. This is the author's version which has not been fully edited and content may change prior to final publication. Citation information: DOI 10.1109/LRA.2024.3396369

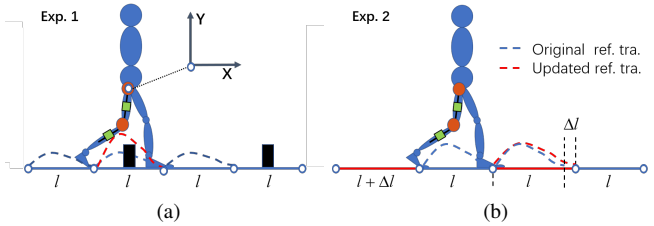

Fig. 7. Schematics of the two sets of experiments. The orange points represent the motors, and the green squares indicate the force sensors. The coordinate origin is set at the hip joint. (a) Illustration of the variable step height walking experiment to cross obstacles, where the obstacles are cuboids with a height of 15 cm. The fixed step length l is 50 cm. (b) Illustration of the variable step length walking experiment, where Δl is 10 cm.

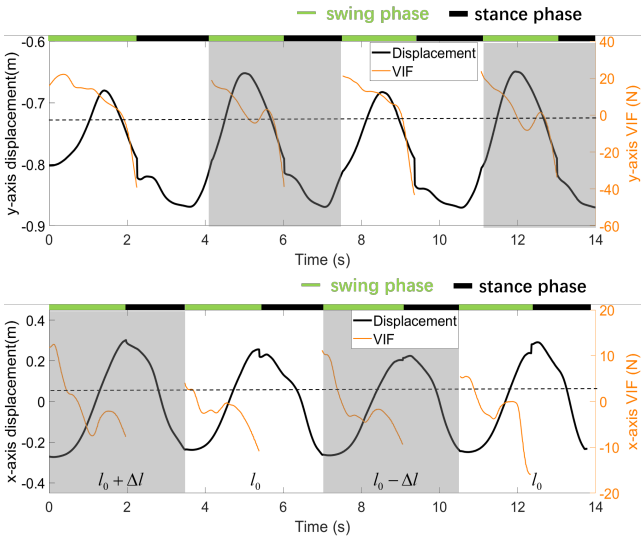

Fig. 8. The displacement of the ankle joint and the corresponding virtual interaction forces from the two sets of experiments. The gray area represents the presence of human-robot interaction tasks, while the dashed line refers to where the VIF equals zero. Since this study does not consider physical human-robot interaction during the stance phase, the interaction force during that period is not displayed.

D. Results and Discussion

Fig. 8 illustrates the virtual interactive forces and the displacement of the LLRR during Exp. 1 and 2 when employing HTDA as the human-robot interaction algorithm. During the swing phase, the interaction algorithm takes effect and updates the reference trajectory based on the virtual interactive forces. The trajectory adjustment is presented as gait height changes in Exp. 1 and gait length alternations in Exp. 2. As the reference trajectory is updated, the confrontation between the subject and the robot diminishes, resulting in a virtual interactive force reduction. Note that at the transition from the swing to the stance phase, the virtual interactive forces exhibit higher absolute values due to the ground impacts. However, this period is relatively short and has a minimal impact on the overall shape of the trajectory.

Preliminary analysis of the experimental data shows that there are significant differences in the absolute values among different subjects. Therefore, relative values are utilized to obtain better insights from the data. Consequently, the results

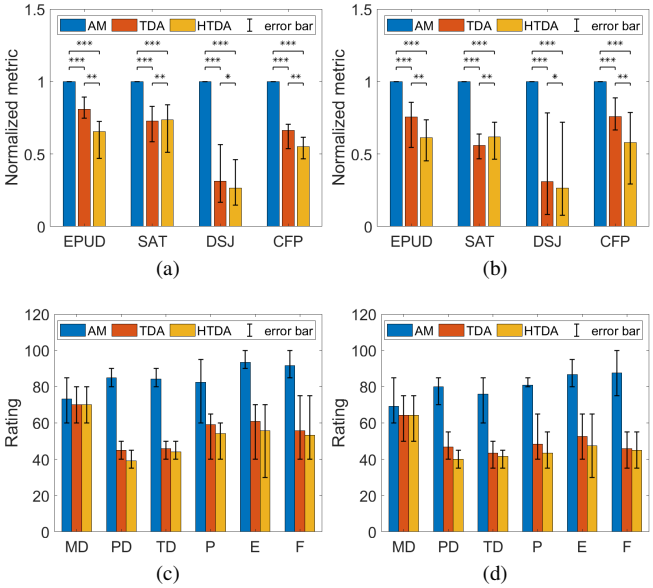

Fig. 9. Results of Exp. 1 and Exp. 2 based on different evaluation metrics. Each plot shows the mean value among subjects using AM (blue), TDA (orange) and HTDA (yellow) as the pHRI algorithm. The asterisks (*), (**) and (***) denote the p-value in t-test satisfies $p \leq 0.05$, $p \leq 1.0 \times 10^{-2}$, and $p \leq 1.0 \times 10^{-3}$, respectively. Error bars indicate the standard error. (a) and (b) are the results of Exp. 1 and Exp. 2, respectively. (c) and (d) are the corresponding NASA TLX scale ratings averaged by fields across all subjects: Mental Demand (MD); Physical Demand (PD); Temporal Demand (TD); Performance (P); Effort (E); Frustration (F).

from using AM are used as the reference to scale the results from using TDA and HTDA. Fig. 9a and 9b illustrates the normalized performance of different algorithms in Exp. 1 and 2, respectively. Compared to AM, HTDA can yield reduced EPUD, SAT, DSJ and CFP by 36.6%, 32.2%, 73.6% and 43.5%, respectively. Compared to TDA, HTDA can yield reduced EPUD, DSJ and CFP by 18.9%, 15.4% and 20.4%, respectively. Note that the SAT values of HTDA and TDA are statistically equivalent, but lower than that of AM. All these mean that the proposed HTDA can effectively respond to the subject's motion intention during active rehabilitation.

Fig. 9c and 9d show the NASA TLX ratings in Exp. 1 and Exp. 2. Compared to AM, HTDA significantly reduced all NASA TLX ratings except Mental Demand (MD). Compared to TDA, HTDA successfully reduced Physical Demand (PD) and Effort (E). This demonstrates that the active control framework using HTDA can balance the control framework's effectiveness and the physiological and psychological burden experienced by the subjects during human-robot interaction.

IV. Conclusion

This paper presents an active control framework for lower limb rehabilitation that combines a hierarchical trajectory deformation algorithm and a hybrid assist-as-needed controller. The HTDA utilizes virtual interaction forces during pHRI to smoothly update the reference trajectory, which is then sent to the hybrid controller to eventually generate the required assistance. As this updated trajectory aligns with the subject's movement intention, the hybrid controller can achieve active

lower limb rehabilitation assistance with reduced human-robot confrontation. The experimental results demonstrate that compared to AM and TDA, HTDA can effectively improve the robot's performance according to metrics such as EPUD, DSJ and CFP. It can potentially be implemented to rehabilitation other than lower limbs in the future [33].

Despite the progress made in this paper, there are still limitations that can be addressed in the future. Firstly, the proposed method uses the virtual interaction forces to generate trajectory deformation, however, the forces may not fully accurately reflect the intention of human subjects during the process. Secondly, the experiments in this paper were conducted only on flat surfaces, without considering trajectory deformation under the constraints of complex terrains. In the future, we will attempt to add biological signals into the framework to more accurately estimate human motion intentions. As with complex terrains, we will consider using terrain information to constrain the human-robot interaction, in hope of balancing safety and interactivity in such scenarios.

REFERENCES

[1] S. Maeshima, A. Osawa, Y. Miyazaki, Y. Seki, C. Miura, Y. Tazawa, and N. Tanahashi, "Influence of dysphagia on short-term outcome in patients with acute stroke," *American Journal of Physical Medicine & Rehabilitation*, vol. 90, no. 4, pp. 316–320, 2011.

[2] G. DeJong, S. D. Horn, B. Conroy, D. Nichols, and E. B. Healton, "Opening the black box of poststroke rehabilitation: stroke rehabilitation patients, processes, and outcomes," *Archives of physical medicine and rehabilitation*, vol. 86, no. 12, pp. 1–7, 2005.

[3] M. Ochi, F. Wada, S. Saeki, and K. Hachisuka, "Gait training in subacute non-ambulatory stroke patients using a full weight-bearing gait-assistance robot: A prospective, randomized, open, blinded-endpoint trial," *Journal of the neurological sciences*, vol. 353, no. 1-2, pp. 130–136, 2015.

[4] M. R. Tucker, J. Olivier, A. Pagel, H. Bleuler, M. Bouri, O. Lambercy, J. d. R. Millán, R. Riener, H. Vallery, and R. Gassert, "Control strategies for active lower extremity prosthetics and orthotics: a review," *Journal of neuroengineering and rehabilitation*, vol. 12, no. 1, pp. 1–30, 2015.

[5] R. Riener, L. Lunenburger, S. Jezernik, M. Anderschitz, G. Colombo, and V. Dietz, "Patient-cooperative strategies for robot-aided treadmill training: first experimental results," *IEEE transactions on neural systems and rehabilitation engineering*, vol. 13, no. 3, pp. 380–394, 2005.

[6] S. K. Banala, S. H. Kim, S. K. Agrawal, and J. P. Scholz, "Robot assisted gait training with active leg exoskeleton (alex)," *IEEE transactions on neural systems and rehabilitation engineering*, vol. 17, no. 1, pp. 2–8, 2008.

[7] G. Colombo, M. Joerg, R. Schreier, V. Dietz *et al.*, "Treadmill training of paraplegic patients using a robotic orthosis," *Journal of rehabilitation research and development*, vol. 37, no. 6, pp. 693–700, 2000.

[8] Z. Warraich and J. A. Kleim, "Neural plasticity: the biological substrate for neurorehabilitation," *Pm&r*, vol. 2, no. 12, pp. S208–S219, 2010.

[9] L. L. Cai, A. J. Fong, C. K. Otoshi, Y. Liang, J. W. Burdick, R. R. Roy, and V. R. Edgerton, "Implications of assist-as-needed robotic step training after a complete spinal cord injury on intrinsic strategies of motor learning," *Journal of Neuroscience*, vol. 26, no. 41, pp. 10 564–10 568, 2006.

[10] C. Caulcrick, W. Huo, E. Franco, S. Mohammed, W. Hoult, and R. Vaidyanathan, "Model predictive control for human-centred lower limb robotic assistance," *IEEE Transactions on Medical Robotics and Bionics*, vol. 3, no. 4, pp. 980–991, 2021.

[11] A. U. Pehlivan, D. P. Losey, and M. K. O'Malley, "Minimal assist-as-needed controller for upper limb robotic rehabilitation," *IEEE Transactions on Robotics*, vol. 32, no. 1, pp. 113–124, 2015.

[12] A. Duschau-Wicke, A. Caprez, and R. Riener, "Patient-cooperative control increases active participation of individuals with sci during robot-aided gait training," *Journal of neuroengineering and rehabilitation*, vol. 7, no. 1, pp. 1–13, 2010.

[13] I. Cervantes, R. Kelly, J. Alvarez-Ramirez, and J. Moreno, "A robust velocity field control," *IEEE Transactions on Control Systems Technology*, vol. 10, no. 6, pp. 888–894, 2002.

[14] A. Martinez, B. Lawson, C. Durrough, and M. Goldfarb, "A velocity-field-based controller for assisting leg movement during walking with a bilateral hip and knee lower limb exoskeleton," *IEEE Transactions on Robotics*, vol. 35, no. 2, pp. 307–316, 2018.

[15] Y. Cao, X. Chen, M. Zhang, and J. Huang, "Adaptive position constrained assist-as-needed control for rehabilitation robots," *IEEE Transactions on Industrial Electronics*, vol. 71, no. 4, pp. 4059–4068, 2024.

[16] Y. Zhang, S. Li, K. J. Nolan, and D. Zanotto, "Adaptive assist-as-needed control based on actor-critic reinforcement learning," in *2019 IEEE/RSJ International Conference on Intelligent Robots and Systems (IROS)*, 2019, pp. 4066–4071.

[17] Y. Li and S. S. Ge, "Human–robot collaboration based on motion intention estimation," *IEEE/ASME Transactions on Mechatronics*, vol. 19, no. 3, pp. 1007–1014, 2013.

[18] H. J. Asl, M. Yamashita, T. Narikiyo, and M. Kawanishi, "Field-based assist-as-needed control schemes for rehabilitation robots," *IEEE/ASME Transactions on Mechatronics*, vol. 25, no. 4, pp. 2100–2111, 2020.

[19] F. Ferraguti, C. Talignani Landi, L. Sabattini, M. Bonfe, C. Fantuzzi, and C. Secchi, "A variable admittance control strategy for stable physical human–robot interaction," *The International Journal of Robotics Research*, vol. 38, no. 6, pp. 747–765, 2019.

[20] J. Zhou, Z. Li, X. Li, X. Wang, and R. Song, "Human–robot cooperation control based on trajectory deformation algorithm for a lower limb rehabilitation robot," *IEEE/ASME Transactions on Mechatronics*, vol. 26, no. 6, pp. 3128–3138, 2021.

[21] J. Yang, D. Huang, J. Xia, and Y. Li, "Trajectory deformation with constrained optimization for bilateral rehabilitation robots," *IEEE/ASME Transactions on Mechatronics*, 2023.

[22] D. P. Losey and M. K. O'Malley, "Trajectory deformations from physical human–robot interaction," *IEEE Transactions on Robotics*, vol. 34, no. 1, pp. 126–138, 2017.

[23] L.-L. Li, G.-Z. Cao, H.-J. Liang, Y.-P. Zhang, and F. Cui, "Human lower limb motion intention recognition for exoskeletons: A review," *IEEE Sensors Journal*, 2023.

[24] X. Yu, W. He, Y. Li, C. Xue, J. Li, J. Zou, and C. Yang, "Bayesian estimation of human impedance and motion intention for human–robot collaboration," *IEEE transactions on cybernetics*, vol. 51, no. 4, pp. 1822–1834, 2019.

[25] K. I. Alevizos, C. P. Bechlioulis, and K. J. Kyriakopoulos, "Physical human–robot cooperation based on robust motion intention estimation," *Robotica*, vol. 38, no. 10, pp. 1842–1866, 2020.

[26] Y. Li and S. S. Ge, "Human-robot collaboration based on motion intention estimation," *IEEE/ASME Transactions on Mechatronics*, vol. 19, no. 3, pp. 1007–1014, 2014.

[27] R. Chipalkatty, G. Droge, and M. B. Egerstedt, "Less is more: Mixed-initiative model-predictive control with human inputs," *IEEE Transactions on Robotics*, vol. 29, no. 3, pp. 695–703, 2013.

[28] A. D. Dragan, "Legible robot motion planning," Ph.D. dissertation, Carnegie Mellon University, 2015.

[29] K. H. Lee, S. G. Baek, H. J. Lee, H. R. Choi, H. Moon, and J. C. Koo, "Enhanced transparency for physical human-robot interaction using human hand impedance compensation," *IEEE/ASME Transactions on Mechatronics*, vol. 23, no. 6, pp. 2662–2670, 2018.

[30] J. Choi, B. Na, P.-G. Jung, D.-w. Rha, and K. Kong, "Walkon suit: A medalist in the powered exoskeleton race of cybathlon 2016," *IEEE Robotics & Automation Magazine*, vol. 24, no. 4, pp. 75–86, 2017.

[31] "Cybathlon 2020 global edition - exo finals," https://www.youtube.com/watch?v=mIbaOjXYxHs, accessed: 2023-11-10.

[32] S. G. Hart and L. E. Staveland, "Development of nasa-tlx (task load index): Results of empirical and theoretical research," in *Advances in psychology*. Elsevier, 1988, vol. 52, pp. 139–183.

[33] M. Sui, Y. Ouyang, H. Jin, Z. Chai, C. Wei, J. Li, M. Xu, W. Li, L. Wang, and S. Zhang, "A soft-packaged and portable rehabilitation glove capable of closed-loop fine motor skills," *Nature Machine Intelligence*, vol. 5, no. 10, pp. 1149–1160, 2023.